

# On Numerical Techniques for Determination of the Sonic Point in Unsteady Inviscid Shock Reflections

Ali Hakkaki-Fard\* and Evgeny Timofeev

Department of Mechanical Engineering, McGill University, 817 Sherbrooke West, Montreal, Quebec H3A0C3, Canada

## Abstract

In this paper, three techniques for determination of the sonic/catch-up points in unsteady shock reflections based on numerical flowfield analysis are considered: the Mach-number-based technique, the characteristic-based technique, and the perturbation technique. These techniques are compared using the problem of shock reflection from a convex cylinder simulated with an inviscid, non-heat-conducting flow model and an ideal reflecting surface. It is shown that the sonic points obtained with the Mach-number or characteristic-based techniques, coincide with the catch-up point obtained by the perturbation technique. The obtained sonic point converges to the theoretical sonic point given by the steady two-shock theory as the grid is refined. Quantitative data are presented, which show that very fine meshes are needed to approach the theoretical value with good accuracy. Furthermore, potential sources of significant experimental errors when applying the perturbation technique in shock-tube experiments are identified.

## 1. INTRODUCTION

The sonic point is prominent in the theory of regular-to-Mach reflection transition as one of its possible criteria [1]. When a moving planar shock wave strikes a convex surface (or a curved shock encounters a straight surface or the plane of symmetry) it reflects from it. If the initial type of reflection is the regular one, as the incident shock wave propagates further, at one particular shock position corresponding to the *sonic point* the flow on the surface just behind the reflected shock becomes sonic with respect to the reflection point. Then, downstream perturbations can reach the reflection point and, supposedly, may initiate the regular-to-Mach reflection transition.

It is not easy to determine the location of the sonic point experimentally. A direct method would require continuous monitoring of flow parameters (velocity, temperature) just behind the reflected shock. Another, more feasible, way is based on tracking of very weak (not altering essentially the flow under study) waves generated by sources on the boundary of the flow domain. In case of shock wave reflection/diffraction, the shock wave itself may produce weak perturbation signals when passing over small geometrical features on the wall (e.g., minute bumps or grooves). These perturbations propagate outward in all directions with the signal speed, which is the local sound speed plus the local flow velocity. This approach represents another way to find the sonic point because the downstream perturbations can be communicated to the reflection point only if the sonic point has been reached. The sonic point found using weak perturbation tracking may be also called the *catch-up point* because its location is determined from the ability of downstream disturbances to catch-up with the reflection point.

Lock and Dewey [2] were among the earliest researchers who applied an experimental diagnostics technique using weak waves in order to evaluate the sonic criterion for rigid inclined surfaces. Skews and Kleine [3] expanded the diagnostics technique based on the tracking of weak perturbations in combination with high speed time-resolved imaging, to a wide variety of shock wave flows. In a recent experimental study [4], they used this diagnostics to detect the catch-up point on convex cylinders. They generated weak perturbations on the surface of circular cylinders with minute grooves and tracked them using high speed time-resolved optical imaging. In this way, they were able to identify the

---

\*Corresponding Author. E-mail: ali.hakkaki-fard@mail.mcgill.ca; evgeny.timofeev@mcgill.ca

moment and the point on the cylinder surface when and where the disturbances for the first time catch up with the reflection point. They found that on a convex circular arc the catch-up point is reached at a higher wall angle than in the case of a wedge (in which case it is close to the steady-state two-shock-theory value for the sonic point). Thus, the relationship between this experimentally-observed *catch-up point* and the *sonic point* is not immediately obvious. In general, it is useful to distinguish the sonic point and the catch-up point unless it is proven that they are the same points indeed.

In numerical simulations, the range of options for sonic point determination is wider because all flow parameters are available at any moment and location. The main goal of the present paper is to consider and compare various techniques to determine the sonic points from numerical flowfields, namely, the Mach-number-based technique, the characteristic-based technique, and the perturbation technique. The first, Mach-number-based, technique implies direct application of the sonic point definition when analyzing Mach number distribution on the cylinder surface [5]. The second, characteristic-based, technique assumes that the sonic point is reached when the characteristic speed  $u + c$  just behind the reflection point is equal or greater than the speed of the reflection point motion along the reflecting surface. Finally, the third technique may be considered as a numerical implementation of the perturbation technique by Skews & Kleine [4] but with infinitesimally weak perturbations.

Theoretically, when considering shocks as discontinuities in inviscid flowfields, all these three ways are gas-dynamically equivalent. However, the flowfields produced by numerical simulations differ from the idealized picture: shocks and other discontinuities are smeared due to numerical viscosity; the reflection point actually becomes a “reflection zone” where two smeared fronts intersect (see Fig. 1b). Even when using quasi-monotone shock-capturing schemes, low amplitude oscillations (“numerical noise”) is present in the solutions. Therefore, it is of importance to apply the above techniques to actual numerical flowfields and evaluate their results. The results for *inviscid* numerical simulations of a test problem with different grid resolutions are presented in this paper and compared with the two-shock theory predictions.

Shock reflection from a convex cylinder is chosen here as a test problem for comparison of the above-mentioned techniques. The schematic illustration of the problem is presented in Fig. 1a with the aim to introduce the angle-related terminology used in this paper. In this figure, the *cylinder angle* indicates the position of the incident shock wave along the surface of the cylinder in terms of polar angle counted from the horizontal direction clockwise; the *incident angle* is the angle between the incident shock wave and the tangential line to the surface of the cylinder (it is equal to the cylinder angle); the *initial angle of incidence* is the incident angle when the incident shock wave strikes the surface of the cylinder for the first time; and the *wall angle* (also called the *wedge angle*) is the angle between the tangential line to the surface of the cylinder and the horizontal line.

The two-dimensional computations are performed using a locally adaptive unstructured unsteady Euler code [6, 7], which is based on a second order in space and time, MUSCL-type, TVD finite-volume solver. The computational domain is discretized with an unstructured mesh composed of triangular grid elements, which is adapted to the solution in the course of computation using a sensor based on the normalized second derivative of density. The grid refinement is based on the classical transient reversible *h*-refinement procedure.

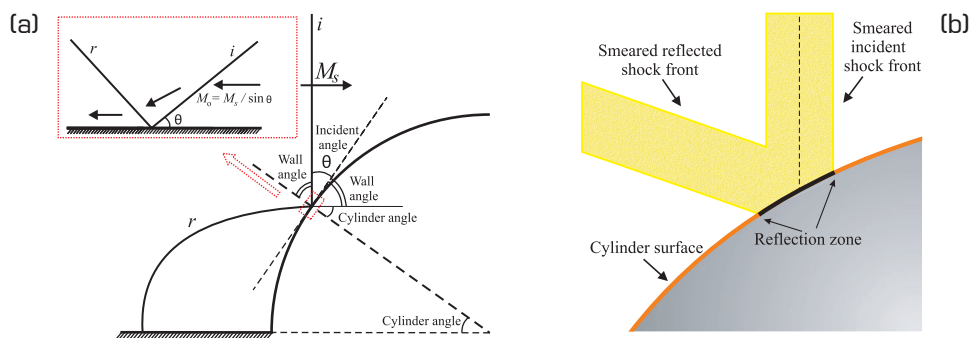


Figure 1. (a) Schematics of regular shock reflection from a convex cylinder with the illustration of the local Galilean transformation into the frame of reference attached to the reflection point:  $i$  and  $r$  represent the incident and reflected shock waves; (b) Schematics of typical numerical representation of the regular shock reflection pattern.

The remainder of the paper is organized as follows. Details of the three techniques for determination of the sonic/catch-up point are described in Section 2. In the next Section 3 the results of their application to numerical flowfields with different grid resolution are provided and discussed. Further discussion is given in the concluding Section 4.

## 2. SONIC/CATCH-UP POINT DETERMINATION TECHNIQUES

### 2.1. The Mach-number-based technique

The Mach-number-based technique implies direct application of the sonic point definition through analysis of the instant Mach number distribution on the cylinder surface. According to the definition of the sonic point, it is the point at which the flow behind the reflected shock becomes sonic with respect to the reflection point. The reflection point moves along the cylinder surface with the velocity  $D = V_s / \sin \theta$ , where  $V_s$  is the incident shock velocity ( $V_s = M_s c_0$  with  $M_s$  being the incident shock Mach number and  $c_0$  – the speed of sound in front of the incident shock) and  $\theta$  is the cylinder angle corresponding to the current location of the incident shock. If  $u_\tau$  denotes the tangential flow velocity on the cylinder surface, then  $D - u_\tau$  would be the tangential flow velocity relative to the reflection point. The division by the speed of sound  $c$  at the same location results in the local relative flow Mach number  $M$ . Therefore, in order to find the sonic point the flow Mach number distribution on the cylinder surface (in the frame of reference attached to the reflection point) should be analyzed. That is why this method is called the *Mach-number-based technique*.

At earlier moments, when the sonic point is not reached yet, the flow along the surface in the frame of reference attached to the reflection point is entirely supersonic ( $M > 1$  everywhere). When the sonic point is just reached, a grid node (or nodes) with

$$M = \frac{D - u_\tau}{c} \leq 1 \quad (1)$$

appears at a certain time step, i.e., a small subsonic zone is formed. However, due to the presence of numerical noise in the solution, this subsonic zone may disappear temporarily at the next time step(s) and/or a few other small isolated subsonic zones may appear. It is not clear which moment or spatial location should be designated as the sonic point. In order to overcome this difficulty and to introduce a consistent way of the sonic point determination on different grids, the sonic line evolution can be considered.

Figure 2a shows the incident and reflected shock waves, the sonic line and the subsonic region developed behind the reflected shock wave when the shock has *already passed* the sonic point. Points A and B are the intersections of the sonic line with the cylinder surface. Their locations at each moment can be determined from the Mach number distribution on the cylinder surface in the frame of reference attached to the reflection point. Then the trajectories of points A and B can be plotted together, as shown in Fig. 2b, and traced back in time. Their intersection would give the location of the sonic point, where

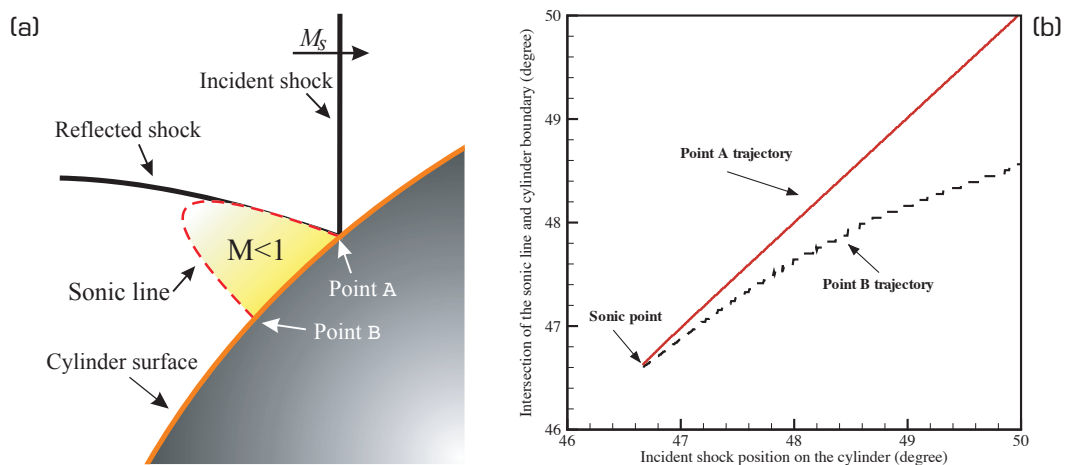


Figure 2. (a) Illustration of the developed sonic line and subsonic region when the incident shock has passed the sonic point; (b) Typical trajectories of points A and B (see Fig. 2a) versus the position of the incident shock [angles on the axes are given in terms of cylinder angle].

the flow right behind the reflection point would become sonic with respect to the reflection point and the subsonic zone would grow afterwards.

## 2.2. The characteristic-based technique

The characteristic-based technique also analyzes flow parameters on the cylinder surface only. Small perturbations propagate along the surface with the velocity  $u_\tau + c$ . The reflection point moves along the cylinder surface with the velocity  $D$  defined above. At the sonic point, downstream disturbances are capable, for the first time, of reaching the reflection point. This is possible only if

$$u_\tau + c \geq D, \quad (2)$$

which becomes the criterion for finding the sonic point. In other words, on an  $x - t$  diagram drawn for the cylinder surface the inverse slope of  $C +$  characteristic should become greater than the inverse slope corresponding to the trajectory of the incident shock along the surface. That is why this technique is called the *characteristic-based technique*. The sonic point location would correspond to the moment (shock location) when the condition (2) is for the first time satisfied downstream of the reflection point. It should be noted that this condition is, in fact, gasdynamically equivalent to the condition (1) of the Mach-number based technique.

Figure 3a illustrates this technique. Three points “a”, “r”, and “b” along the cylinder surface are shown. Point “a” is downstream of the incident shock; point “b” is upstream of it (in the frame of reference attached to the reflection point); and point “r” is the reflection point. In this method, the signal velocities along the cylinder surface downstream of the reflection point (e.g., at point “a”) are compared to the reflection point (“r”) velocity.

In order to find the sonic point using the characteristic-based technique, at each numerical time step relation (2) is checked for all grid nodes on the cylinder surface. Through plotting the position of points that satisfy relation (2) versus the shock position valuable information regarding the sonic point and the subsonic zone can be obtained. Such approach is illustrated in Fig. 3b. The sonic point position is indicated, which represents the first point where relation  $u_\tau + c \geq D$  is satisfied. Moreover, the set of points as a whole represents the subsonic zone developed behind the reflection point. The density of the points in Fig. 3b differs from side to side of the subsonic zone, and that is because of adaptive nature of the mesh used in this study. The side closer to the incident shock wave is more dense while the other side is less dense.

The characteristic-based technique may be also interpreted as a “surface-only” version of the perturbation technique which is explained in the next subsection.

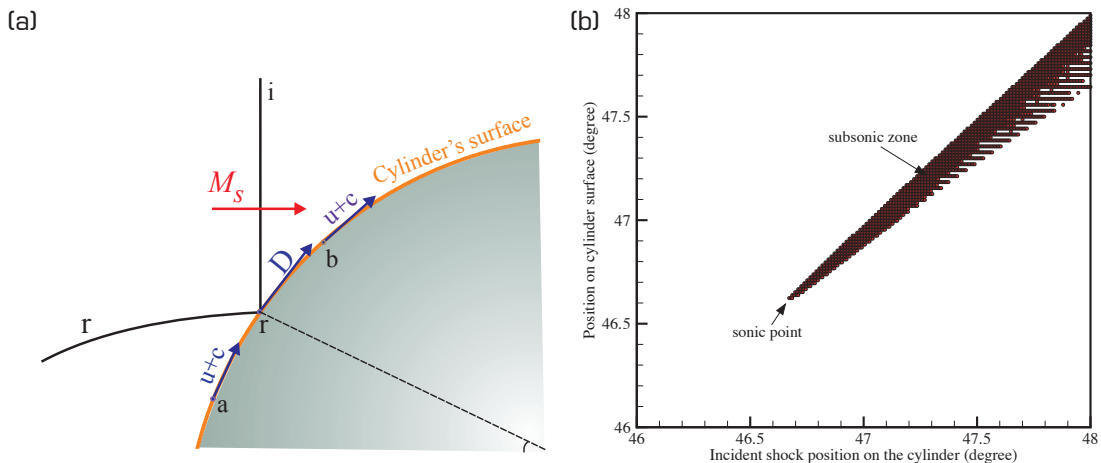


Figure 3. (a) Schematics of the characteristic-based technique; (b) Typical plot resulting from application of the characteristic-based technique (angles on the axes are given in terms of cylinder angle).

### 2.3. The perturbation technique

The idea of the perturbation technique is to observe the propagation of weak disturbances originating on the reflecting surface behind the reflection point and to analyze which of them, and when, are capable of reaching the reflection point. In order to simulate this technique numerically, it is required to generate perturbation signals. One way is to perform the direct numerical modeling of the perturbation technique by Skews and Kleine [4], i.e., to use small perturbation sources, such as small bumps/grooves, on the boundary of the flow domain, similarly to the experimental perturbation sources. Technically, using locally refined unstructured grids, this approach is possible, even though the size of geometrical perturbation sources may be very small (as compared to the radius of cylinder and the general size of the computational domain). However, it would be very challenging and expensive computationally because in order to capture the evolution of the generated very weak waves a very fine mesh and/or higher-order numerical schemes are required.

There is a more efficient approach that implements tracking of imaginary (and therefore, infinitesimally weak) perturbations as a postprocessing procedure performed after each time step of CFD simulation. As soon as the incident shock reaches an imaginary perturbation source the perturbation wave front originating from the source is initiated as a set of points (not related to grid nodes). In order to track these weak perturbation wavefronts the Huygens–Fresnel principle [8] can be applied. After each time step, each point of the wave front is shifted in space according to the local speed of sound and local flow velocity. More details about the numerical perturbation tracking method may be found in [9].

Figure 4a (similar to Fig. 4 of [4]) shows a typical frame of a movie generated from the CFD simulation of the unsteady shock reflection from a convex cylinder with three perturbation sources along the cylinder surface, for an inviscid case. Three perturbation sources labeled as 1, 2 and 3, the forward facing perturbation waves denoted as “*P*” waves, and the backward facing perturbation waves denoted as “*Q*” waves are shown in this figure. Figure 4b presents the positions of various waves on the cylinder surface as a function of the incident shock position for the same simulation. In other words, Fig. 4b is an  $x - t$  diagram of the unsteady flow, with the shock position serving as a time variable. The dash-dotted lines indicate the reflection zone trajectory while dashed lines *P* and *Q* correspond to the forward and backward facing perturbation waves, respectively. In general, by tracking perturbation signals using the movie frames and/or the wave diagram it is possible to identify the moment and the point on the cylinder surface when and where disturbances for the first time catch up with the reflection point, and that represents the essence of the perturbation technique.

Figure 4 allows making an interesting observation. All three backward facing perturbation waves (*Q*<sub>1</sub>, *Q*<sub>2</sub>, and *Q*<sub>3</sub>) can be seen in Fig. 4a and 4b. However, only the first and the second forward facing perturbation waves (*P*<sub>1</sub> and *P*<sub>2</sub>) can be seen in Fig. 4a. The lines representing them on the  $x - t$  diagram (Fig. 4b) clearly diverge from the reflection zone trajectory, which demonstrates that the flow is supersonic relatively to the reflection point behind the reflected shock wave at these two perturbation sources. These perturbations catch up with the reflection zone only much later, after the incident shock has passed the sonic/catch-up point. Furthermore, it appears that the forward facing perturbation wave arising from source “3” (*P*<sub>3</sub>) has caught up and merged with the reflection pattern, and cannot be seen in Fig. 4a. Therefore, it may be concluded that, *judging from this frame*, the catch-up point is reached before this moment. However, careful inspection of Fig. 4b reveals that *P*<sub>3</sub> wave does emerge from the reflection zone, remaining very close to it so that on a movie frame, like that in Fig. 4a, it is indistinguishable from the reflection zone. For inviscid simulations, the reflection zone thickness is determined only by numerical viscosity and, therefore, it is “always” (in fact, within available computer resources) possible to improve accuracy via grid refinement and to resolve and clearly distinguish all the waves, no matter how close they are. However, this observation may have very important implications for interpretation of experimental optical images (with unavoidable finite thickness of all wave fronts due to optical effects). It may happen that the finite thickness of shock wave and disturbance fronts would prevent correct determination of the catch-up point location.

The next section compares numerical results for the location of sonic and catch-up points obtained with the techniques described above.

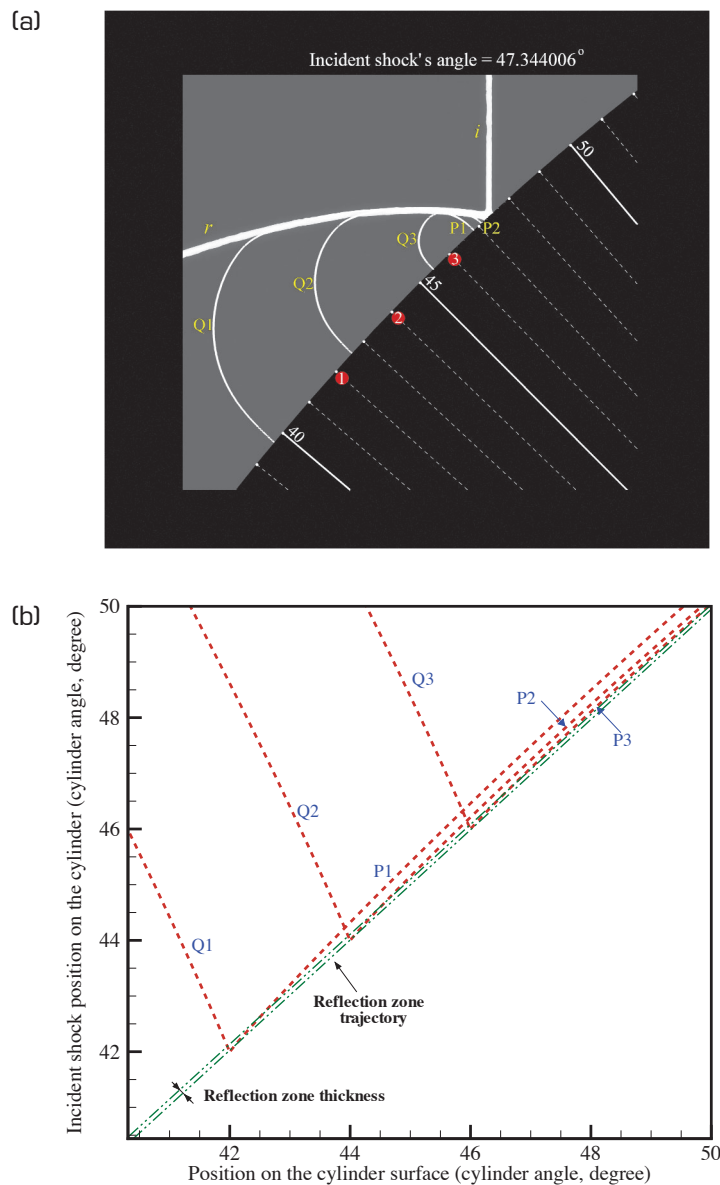


Figure 4. (a) A typical frame from the CFD movie demonstrating the evolution of the incident and reflected shocks as well as three disturbance fronts (their initiation points on the cylinder surface are indicated as red circles); (b) The respective typical wave diagram of shock propagation along the cylinder surface with three forward (P) and backward (Q) facing perturbation waves.

### 3. COMPARISON OF THE SONIC AND CATCH-UP POINTS OBTAINED BY DIFFERENT TECHNIQUES

In the present section, the comparison of different techniques for the determination of *sonic* and *catch-up* points is carried out for the problem of shock wave reflection from a convex cylinder. The numerical simulations are based on an inviscid, non-heat-conducting flow model with an ideal reflecting surface (the impermeable wall boundary condition). The incident shock Mach number  $M_s$  is 1.211, which is one of the Mach numbers used by Skews and Kleins [4] in their experiments. The specific heat ratio  $\gamma$  is equal to 1.4. The initial angle of incidence is  $5^\circ$ , i.e., the cylinder arc begins from the polar angle equal to  $5^\circ$ .

In the subsequent sections all numbers related to linear dimensions are given in terms of the cylinder radius  $R$ , which is used as a scale of distance. In particular, the background mesh size  $\Delta l$  is 0.004, which

approximately corresponds to 250 nodes along the distance equal to the cylinder radius (the mesh size is slightly non-uniform due to unstructured nature of the grid). The grid is refined near solution peculiarities so that each level of refinement reduces the mesh size twice. Therefore, the finest mesh size (near discontinuities) for  $n$  levels of grid refinement may be evaluated as  $\Delta/2^n$ .

### 3.1. The theoretical sonic point

It would also be interesting to compare numerical results with a theoretical prediction of the sonic point. In general, in order to obtain the theoretical sonic point for unsteady problems, the Euler equations for the inviscid case or the Navier-Stokes equations for viscous flow should be solved analytically. As stated by Ben-Dor and Takayama [10], “due to the complexity of the governing equations of unsteady shock reflections, simple transition criteria, such as those presented . . . for steady and pseudo-steady flows, can not be established”. They [11] suggested to divide the unsteady flow into a sequence of momentarily pseudo-steady states and analyze each such state individually using the steady-state shock analysis. Under this assumption, at each moment (or each cylinder angle) inviscid unsteady shock reflection from a convex cylinder can be considered as a pseudosteady shock reflection from the corresponding wedge. Then, by applying the Galilean transformation as shown in Fig. 1a, the corresponding steady problem can be obtained. Then, the oblique shock relations can be applied to solve this two-shock configuration and to find at which angle  $\theta$  the flow behind the reflected shock becomes sonic, i.e., to find the sonic point. The respective formulas may be found in [1]. Therefore, using this approach the sonic point can be predicted using the classical two-shock theory but it is not immediately obvious that the steady-state two-shock theory predictions are valid for the unsteady cases under consideration. The theoretical treatment provides sonic angles as a function of the incident shock Mach number. For the incident shock Mach number equal to 1.211 the sonic angle would be  $45.70^\circ$  (in terms of cylinder angle).

### 3.2. The Mach-number-based technique (sonic point)

The Mach-number-based technique is described in Sec. 2.1. Table 1 presents the sonic angles obtained with this technique for different levels of grid refinement and the finest mesh size used in each simulation. The obtained results show that with increasing the level of refinement, i.e., by refining the grid, the sonic angle converges to the theoretical sonic angle obtained by the two-shock theory.

Figure 5 shows the trajectories of points  $A$  and  $B$  (see Fig. 2a), as well as the trajectory of the reflection zone on the cylinder surface (see Fig. 1b) for the case with 4 grid refinement levels. It is seen that the sonic point and the subsonic region arise behind the reflection zone, and as they develop, the point  $A$  moves into the reflection zone interior. It should be noted that for inviscid simulations the thickness of shock fronts and, therefore, of the reflection zone is not physical in the sense that it would decrease indefinitely with refining the mesh. However, the pattern of trajectories shown in Fig. 5 would remain qualitatively the same for all meshes.

### 3.3. The characteristic-based technique (sonic point)

The characteristic-based technique is described in Sec. 2.2. It turns out that, within the accuracy of two digits after the point, this technique produces exactly the same results as shown in Table 1 for the Mach-number based technique.

**Table 1. Sonic angles obtained by the Mach-number-based technique with different levels of grid refinement for incident shock Mach number of 1.211**

Level of refinement	Finest mesh size (non-dimen.)	Sonic angle (degree)
0	$4.00 \times 10^{-3}$	50.08
2	$1.00 \times 10^{-3}$	47.70
4	$2.50 \times 10^{-4}$	46.66
6	$6.25 \times 10^{-5}$	46.32
8	$1.65 \times 10^{-5}$	46.13
Two-shock theory	45.70	

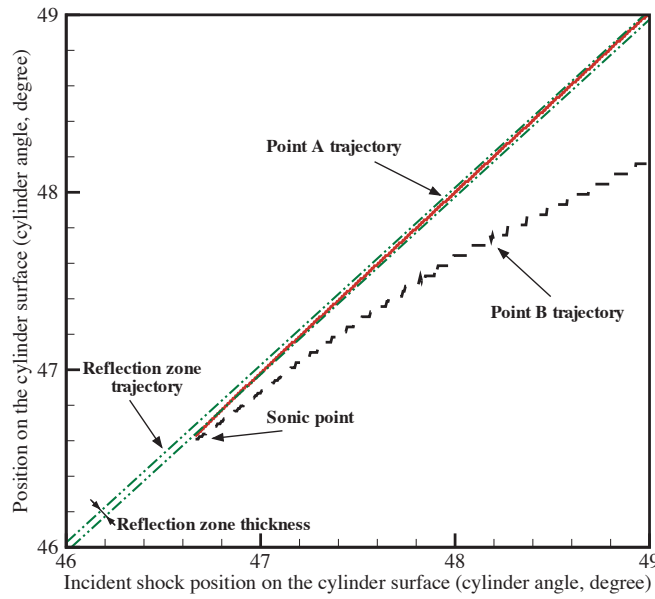


Figure 5. Trajectories of points *A* and *B* versus incident shock position for four levels of grid refinement (the Mach-number-based technique).

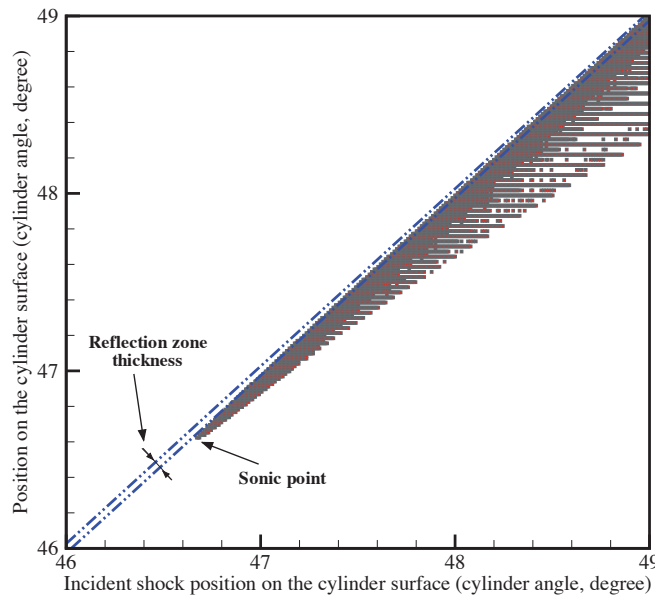


Figure 6. Points (shown by symbols) on the surface of the cylinder that satisfy relation (2) for two levels of grid refinement (the characteristic-based technique).

Figure 6 presents the result obtained with the characteristic-based technique for two levels of grid refinement. The symbols represent the points that satisfy relation (2). The first point that satisfies relation (2) (which is the sonic point) is indicated in the figure. Therefore, the points shown in Fig. 6 represent the zone in which perturbations can propagate faster than or at the same speed as the incident shock moves along the cylinder surface. Similarly to the results obtained with the Mach-number-based technique, Fig. 6 shows that the sonic flow first arises behind the reflection zone and further development of the subsonic zone is very close to that seen in Fig. 5.

### 3.4. The perturbation technique (catch-up point)

The perturbation technique is described in Sec. 2.3. As the catch-up point can be determined either visually from the frames of a CFD movie or by considering the wave diagram, the results are divided into two respective subsections. In all cases two sets of perturbation sources are considered to investigate the effect of their distribution on perturbation technique results. In one case, all perturbation sources are at the odd cylinder angles, such as  $41^\circ$ ,  $43^\circ$ , etc., while in the other case the perturbation sources are at the even cylinder angles, such as  $40^\circ$ ,  $42^\circ$ , etc. There is a 2 degrees distance between two consecutive perturbation sources in both cases.

#### 3.4.1. Applying wave diagram

In the present section, the catch-up point is obtained with the wave diagram. An example of such a diagram is presented in Fig. 4b. By tracking “*P*” waves it is possible to determine the catch-up point. As it is shown in Fig. 4b, “*P*” waves diverge from the shock trajectory at the beginning, but as they enter the subsonic zone, they come back to the shock wave front. It should be noted that as the location of a disturbance source approaches the catch-up point, the respective *P*-wave trajectories become very close to the shock trajectory, so that it becomes difficult to distinguish them (Fig. 4b). If a disturbance source would be located exactly at the catch-up point or at higher cylinder angles, its *P*-wave trajectory would be indistinguishable from the shock trajectory. In other words, at or after the catch-up point, *P*-waves catch-up with the shock wave immediately, by the definition of the catch-up point. As demonstrated in Fig. 4b, just prior to the catch-up point, *P*-wave trajectories run very close to the shock trajectory over a relatively long distance (a few degrees). That results in difficulties in the determination of the catch-up point location. It is suggested to identify as the catch-up point the point where the maximum deviation of the last (closest to the incident shock) resolved *P*-wave trajectory from the shock wave trajectory is observed, as schematically illustrated in Fig. 7. Indeed, at the moment when the maximum deviation of the *P*-wave trajectory and the incident shock wave is achieved, the speed of *P*-wave just equals that of the shock and right thereafter it exceeds the shock wave speed, i.e. the distance between the shock and the *P*-wave begins decreasing. That is only possible if the sonic point has just been reached.

The catch-up points obtained with this technique are presented in Table 2, for odd and even perturbation sources. As can be seen, the results are very close, which means that the perturbation source positions are not overly important for this technique. It should be noted that here perturbation fronts are assumed to have an infinitesimally small thickness, while on experimental schlieren images, perturbation fronts have a finite thickness determined by the properties of the optical set-up. This finite thickness may affect the accuracy of catch-up point determination from the wave diagram obtained via extraction of wave positions from experimental movie frames.

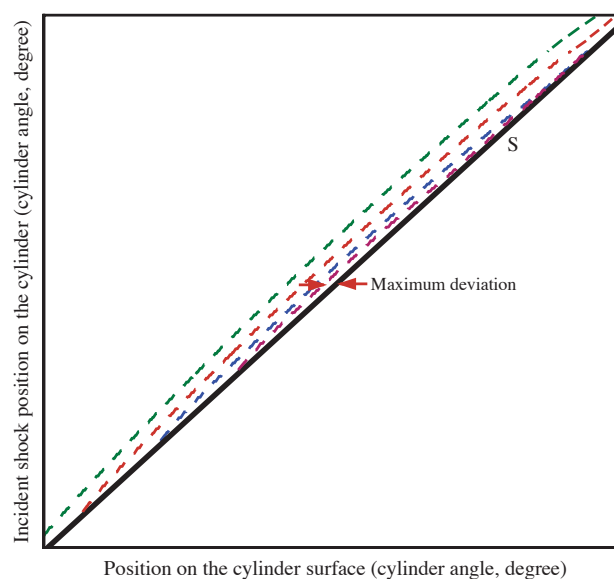


Figure 7. Illustration of the wave diagram and the "maximum deviation" principle. *S* indicates the incident shock trajectory.

**Table 2. Catch-up angles obtained with the perturbation technique (wave diagram) for different levels of grid refinement and incident shock Mach number of 1.211**

Level of refinement	Finest mesh size (non-dimen.)	Catch-up angle (Odd sources)	Catch-up angle (Even sources)
0	$4.00 \times 10^{-3}$	49.82	49.82
2	$1.00 \times 10^{-3}$	47.66	47.66
4	$2.50 \times 10^{-4}$	46.66	46.80
6	$6.25 \times 10^{-5}$	46.50	46.44
8	$1.65 \times 10^{-5}$	46.39	46.23

**Table 3. Catch-up and sonic angles obtained by the perturbation technique (wave diagram), the characteristic-based technique and the Mach-number-based technique for different levels of grid refinement and incident shock Mach number of 1.211**

Levels of refinement	Finest mesh size (non-dimen.)	Catch-up angle (Perturbation tech.) (Wave diagram)	Sonic angle (Characteristic-based tech.)	Sonic angle (Mach-number-based tech.)
0	$4.00 \times 10^{-3}$	49.82	50.08	50.08
2	$1.00 \times 10^{-3}$	47.66	47.70	47.70
4	$2.50 \times 10^{-4}$	46.73	46.66	46.66
6	$6.25 \times 10^{-5}$	46.47	46.32	46.32
8	$1.65 \times 10^{-5}$	46.31	46.13	46.13
Two-shock theory			45.70	

In order to compare these results with the previous methods, the results obtained with different techniques are presented together in Table 3. As the obtained results for odd and even sources are very close, their arithmetical averages are used in Table 3 as the perturbation technique results. Table 3 reveals that the results obtained with these techniques are very close. Hence, it can be concluded that the catch-up point and the sonic point are actually the same points in this inviscid simulation.

### 3.4.2. Visual identification from the movie

In the present section, the catch-up point is obtained visually from the CFD movies via observations where the perturbation signals merge with the reflection point. Therefore, the thickness of shock and perturbation wave fronts may affect the obtained results. Figure 8 illustrates a typical frame of the movie generated with 6 levels of grid refinement. As can be seen, “P1” and “P2” waves are visible, while “P3” and “P4” have already merged with the reflection pattern, which means, *judging from this frame only*, that the catch-up point is somewhere between source “2” and the current shock position. In fact, signals “P3” and “P4” are not seen in all earlier frames as well, which leads to the conclusion that the catch up point should be between sources “2” and “3”.

Table 4 presents the results for odd and even perturbation sources. The values given in the parentheses correspond to the location of two perturbation sources. For the *second* source its perturbation P-wave is not visible in the movie at all, i.e., this disturbance catches up with the reflection point immediately (at its origin). The first source precedes the second one and its P-wave is identifiable in the movie. Therefore, the catch-up point is somewhere between these two points, e.g., it can be approximated to be at their arithmetical average. The results presented in Table 4 reveal that the catch-up point obtained visually from the simulation movie occurs at smaller cylinder angles, and also that the perturbations source positions affect the visually determined catch-up point.

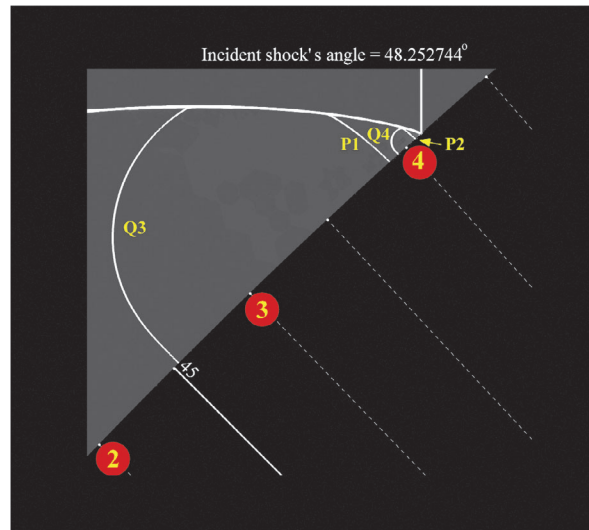


Figure 8. Typical frame of the simulation movie for disturbance sources at even angles, with six levels of grid refinement.

**Table 4. Catch-up angles obtained by the perturbation technique via visual inspection of the simulation movies**

Levels of refinement	Finest mesh size (non-dimen.)	Catch-up angle (Odd sources)	Catch-up angle (Even sources)
0	$4.00 \times 10^{-3}$	44 (43–45)	43 (42–44)
2	$1.00 \times 10^{-3}$	44 (43–45)	45 (44–46)
4	$2.50 \times 10^{-4}$	44 (43–45)	45 (44–46)
6	$6.25 \times 10^{-5}$	44 (43–45)	45 (44–46)

#### 4. CONCLUDING REMARKS

Determination of the sonic/catch-up point in an unsteady flowfield is an important aspect in the studies of shock reflection. In this regard three techniques for determination of the sonic/catch-up points in unsteady shock reflections based on numerical flow-field analysis are introduced and compared in this paper. The results of inviscid numerical simulations of the test problem with different grid resolutions show that the sonic points obtained with the Mach-number or characteristic-based techniques, coincide with the catch-up point obtained by the perturbation technique (even when using a finite number of perturbation sources).

The obtained sonic point converges to the theoretical sonic point given by the steady two-shock theory as the grid is refined. It is remarkable how fine the mesh should be to approach the theoretical value within just  $0.5^\circ$  or 1% accuracy (good accuracy but not something extraordinary). One may have false impression that it is easier to obtain accurate values for the sonic point location as compared to the location of the RR-MR transition, which is known to be notoriously difficult to resolve (see [12]) because the trajectory of the triple point is tangential to the cylinder surface. However, the results of the present paper show clearly that it is not the case.

It is worth noting that if the numerical modeling were conducted using the Navier-Stokes flow model, only the perturbation technique can be used to obtain the location of the catch-up point from numerical results. Under the no-slip boundary condition, the flow velocity on a solid wall is always zero, thus making it impossible to apply the Mach-number-based and characteristic-based techniques, which analyze the data on the solid surface only. In this case, the relative flow velocity on the solid surface always remain supersonic relatively the reflection point and the sonic point does not occur on it.

The perturbation technique can be used as a powerful tool for determination of the sonic/catch-up point in future studies when the Mach-number-based or characteristic-based techniques are not

applicable. The present work also reveals potential source of experimental errors when applying the perturbation technique. It is shown that close to the sonic point the trajectories of the incident shock (or the reflection zone) and the perturbation signals are nearly parallel and high numerical resolution is needed to distinguish them. On experimental images the shock and perturbation fronts have a finite optical thickness, which may be significant, especially for high speed movies which typically have lower resolution than still images. This may lead to difficulties in determination whether or not a particular disturbance has already merged with the reflection point. It may be conjectured that this type of error may be the reason why the catch-up point obtained experimentally by Skews and Kleine is well ahead (at higher wedge angles) than the theoretical sonic point. However, further numerical studies, in particular using the Navier-Stokes equations, are needed to finally resolve the issue with confidence.

### ACKNOWLEDGEMENTS

The present study is supported in part by the NSERC Discovery grant RGPIN/298232-2009 and the FQRNT Team grant PR-126114.

### REFERENCES

- [1] Ben-Dor, G., "Shock wave reflection phenomena", Springer, 2<sup>nd</sup> edition, New York, 2007.
- [2] Lock, G. D., and Dewey, J. M., "An experimental investigation of the sonic criterion for transition from regular to Mach reflection of weak shock waves", *Experiments in Fluids*, Vol. 7, pp. 289–292, 1989.
- [3] Skews, B. W., and Kleine, H., "Unsteady flow diagnostics using weak perturbations", *Experiments in Fluids*, Vol. 46, No. 1, pp. 65–76, 2008.
- [4] Skews, B. W., and Kleine, H., "Shock wave interaction with convex circular cylindrical surface", *Journal of Fluid Mechanics*, Vol. 654, pp. 195–205, 2010.
- [5] Hakkaki-Fard, A., and Timofeev, E., "High resolution determination of sonic and detachment angles at shock wave reflection from a circular cylinder", *Proc. 17th Annual Conf. of CFD Society of Canada*, Ottawa, May 3–5, 6p, 2009.
- [6] Drikakis, D., Ofengeim, D., Timofeev, E., and Voinovich, P., "Computation of non-stationary shock-wave/cylinder interaction using adaptive-grid methods", *Journal of Fluids and Structures*, Vol. 11, No. 6, pp. 665–691, 1997.
- [7] Saito, T., Voinovich, P., Timofeev, E., and Takayama, K., "Development and application of high-resolution adaptive numerical techniques in Shock Wave Research Center", In: "Godunov Methods: Theory and Applications", Edited Review, Toro, E.F. (Ed.), Kluwer Academic/Plenum Publishers, New York, USA, 2001, pp. 763–784.
- [8] Longhurst, R. S., "Geometrical and physical optics", 2nd Edition, Longmans, London, 1968.
- [9] Hakkaki-Fard, A., "Study on the sonic point in unsteady shock reflections via numerical flowfield analysis", PhD thesis, McGill University, 2012; <http://digitool.library.mcgill.ca/R/>.
- [10] Ben-Dor, G., and Takayama, K., "The phenomena of shock wave reflection - a review of unsolved problems and future research needs", *Shock Waves*, Vol. 2, No. 4, pp. 211–223, 1992.
- [11] Ben-Dor, G., and Takayama, K., "Application of steady shock polars to unsteady shock wave reflections", *AIAA Journal*, Vol. 24, No. 4, pp. 682–684, 1986.
- [12] Timofeev, E., Skews, B.W., Voinovich, P.A., and Takayama K., "The Influence of unsteadiness and three-dimensionality on regular-to-Mach reflection transitions: a high-resolution study," In: Ball, G.J., Hillier, R., Roberts, G.T. (Eds.), "Shock Waves", Proceedings of the 22th International Symposium on Shock Waves, London, UK, 18–23 July, 1999, University of Southampton, 1999, Vol. 2, pp. 1231–1236.